



OPEN

Superconducting quantum interference at the atomic scale

Sujoy Karan¹, Haonan Huang¹, Ciprian Padurariu², Björn Kubala^{2,3}, Andreas Theiler⁴, Annica M. Black-Schaffer⁴, Gonzalo Morrás⁵, Alfredo Levy Yeyati⁵, Juan Carlos Cuevas⁵, Joachim Ankerhold², Klaus Kern^{1,6} and Christian R. Ast¹✉

A single spin in a Josephson junction can reverse the flow of the supercurrent by changing the sign of the superconducting phase difference across it. At mesoscopic length scales, these π -junctions are employed in various applications, such as finding the pairing symmetry of the underlying superconductor, as well as quantum computing. At the atomic scale, the counterpart of a single spin in a superconducting tunnel junction is known as a Yu-Shiba-Rusinov state. Observation of the supercurrent reversal in that setting has so far remained elusive. Here we demonstrate such a 0 to π transition of a Josephson junction through a Yu-Shiba-Rusinov state as we continuously change the impurity-superconductor coupling. We detect the sign change in the critical current by exploiting a second transport channel as reference in analogy to a superconducting quantum interference device, which provides our scanning tunnelling microscope with the required phase sensitivity. The measured change in the Josephson current is a signature of the quantum phase transition and allows its characterization with high resolution.

Two superconductors that are connected by a weak link can sustain a supercurrent, which is carried by Cooper pairs—the well-known Josephson effect¹. Inserting a single spin into the junction may completely change its behaviour by reversing the direction of the supercurrent², which is the result of a π shift in the phase across the junction. Such π -junctions have been used in finding the pairing symmetry in unconventional superconductors^{3–7}, and they have been proposed as building blocks for energy-efficient quantum computing or high-speed memory^{8–10}. At mesoscopic length scales (~ 10 to 100 nm), π -junctions may be realized by singly occupied quantum dots or ferromagnetic interlayers^{11–18}. At the atomic scale (~ 0.1 nm), a single magnetic impurity, which is exchange-coupled to a superconductor, induces a spin nondegenerate superconducting bound state, a Yu-Shiba-Rusinov (YSR) state^{19–21}. By tuning the magnetic exchange coupling, the YSR state can be driven through a quantum phase transition (QPT) with a concomitant π shift^{22–26}.

The hallmark of this QPT in YSR states is a discontinuous change in the total spin of the respective ground states: a previously free impurity spin turns into a screened spin when the magnetic exchange coupling increases beyond a critical value. Consequently, a reversal in the flow of Cooper pairs through a YSR state has been predicted²⁶. Experimentally, the QPT can be identified by a zero energy crossing of the YSR state in differential conductance spectra^{27–31}. However, the actual consequences for the fundamental Josephson effect remain elusive in atomic-scale junctions.

The observation of a YSR state-based π -junction is experimentally challenging, because detecting such a phase shift between superconducting ground states requires a reference channel. At mesoscopic length scales, this is typically solved by employing a superconducting quantum interference device (SQUID) loop geometry^{14–17}. To reach similar conditions at the atomic scale, a scanning

tunnelling microscope (STM) requires a rudimentary phase sensitivity through an additional transport channel^{15,18}.

In this Article we demonstrate a supercurrent reversal in an atomic-scale Josephson junction through a YSR state as we move across the QPT. We produce a magnetic impurity at the apex of a superconducting vanadium tip (Fig. 1a), which is approached to a superconducting V(100) sample. As we approach, the atomic forces pull on the impurity^{27,28,32–35}, which reduces the impurity-superconductor coupling Γ along with the magnetic exchange coupling (also see Supplementary Section A). This concomitantly allows the YSR state to pass from the strong scattering regime (screened spin) to the weak scattering regime (free spin), as outlined in Fig. 1b. The two scenarios are schematically illustrated in Fig. 1c, where the total spin in the free spin regime is $S_{\text{tot}} = \frac{1}{2}$. In the screened spin regime, a Cooper pair is broken to screen the impurity spin, changing the overall parity of the system (indicating whether the total number of particles is even or odd) as well as the total spin to $S_{\text{tot}} = 0$.

In our experiment, the detection of the supercurrent reversal is only possible by exploiting the parallel presence of a second transport channel featuring a conventional superconducting Bardeen-Cooper-Schrieffer (BCS) gap without any YSR state as a reference channel (Fig. 1a and Methods). The sign change in the supercurrent through the YSR state manifests itself as a step in the measured net Josephson current, resulting from the changeover of a constructive to a destructive interference of the two transport channels across the QPT.

The evolution of the YSR state as a function of the normal state conductance G_N is shown in Fig. 1d. The YSR state moves across the QPT when the YSR energies are closest to each other. Because both tip and sample are superconducting, in the spectrum the tip YSR states appear at voltages V shifted by the sample gap Δ_s , that is, $eV = \varepsilon + \Delta_s$, with the YSR state energy ε varying with the normal

¹Max-Planck-Institut für Festkörperforschung, Stuttgart, Germany. ²Institut für Komplexe Quantensysteme and IQST, Universität Ulm, Ulm, Germany.

³Institute of Quantum Technologies, German Aerospace Center (DLR), Ulm, Germany. ⁴Department of Physics and Astronomy, Uppsala University, Uppsala, Sweden. ⁵Departamento de Física Teórica de la Materia Condensada and Condensed Matter Physics Center (IFIMAC), Universidad Autónoma de Madrid, Madrid, Spain. ⁶Institut de Physique, Ecole Polytechnique Fédérale de Lausanne, Lausanne, Switzerland. ✉e-mail: c.ast@fkf.mpg.de

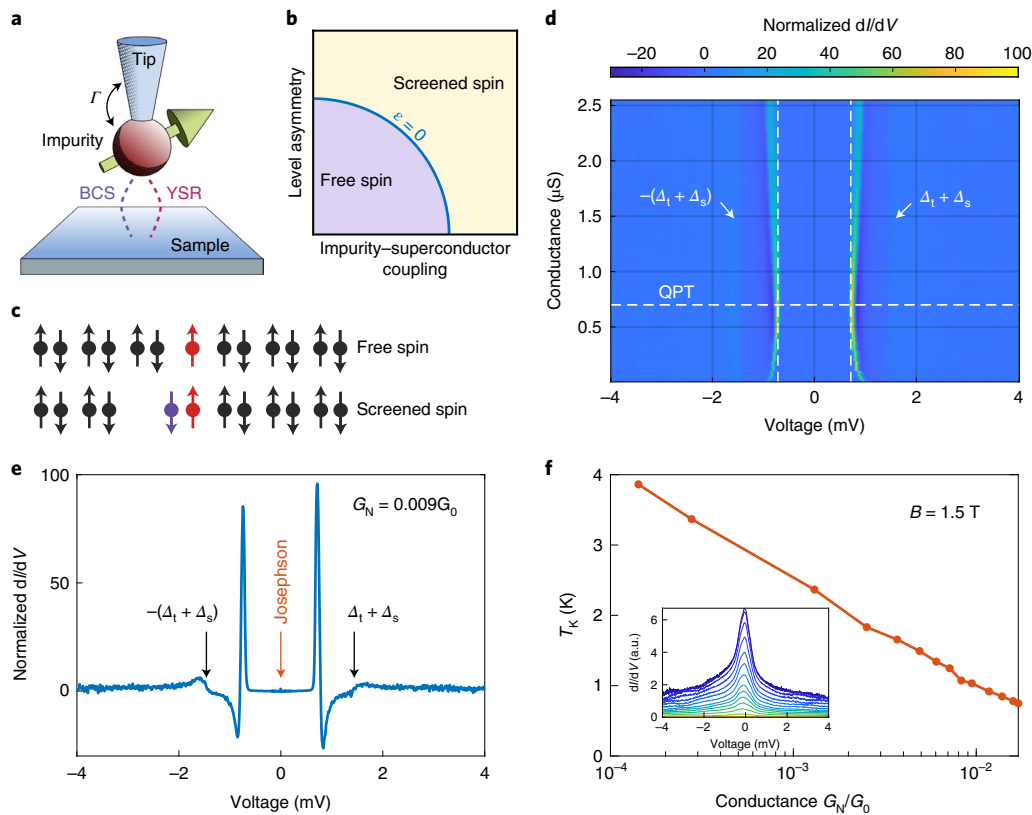


Fig. 1 | Atomic YSR state. **a**, Schematic of the tunnel junction. The YSR impurity is at the tip, with two transport channels (BCS and YSR) indicated as dashed lines. **b**, Phase diagram of the YSR system as function of impurity–superconductor coupling and level (particle-hole) asymmetry. **c**, Schematic of the free spin and the screened spin regime. In the screened regime, a Cooper pair is broken, changing the overall parity of the system. **d**, Differential conductance spectra as a function of bias voltage (x axis) and conductance (y axis). The prominent peaks are the YSR states, and the coherence peaks are only barely visible. The vertical dashed lines indicate the position of the sample gap, Δ_s . **e**, Horizontal line cut through **d** to show the prominent YSR peaks. **f**, Kondo temperature of the Kondo effect in the same junction at a magnetic field of 1.5 T, when superconductivity is quenched. The Kondo spectra are shown in the inset.

state conductance G_N . Interestingly, there are no distinct coherence peaks visible at the sum of the tip gap and the sample gap $\pm(\Delta_t + \Delta_s)$, which indicates that a second transport channel through an empty gap (that is, without any YSR state and hence with coherence peaks) has a much weaker, but still finite transmission compared to the YSR state. This can be more directly seen in a single spectrum near the QPT, which is shown in Fig. 1e. The coherence peaks at $eV = \pm(\Delta_t + \Delta_s)$ are greatly reduced, and the YSR peaks are prominently enhanced by a factor of almost 100.

To confirm that the impurity–superconductor coupling (in our case the impurity–tip coupling) decreases with increasing conductance, we measured the Kondo effect in the same junction by quenching the superconductivity in a magnetic field of 1.5 T. The Kondo spectra are shown in the inset of Fig. 1f, from which we extract the Kondo temperature T_K by fitting the data to numerical renormalization group (NRG) theory calculations (for details see Supplementary Section B). As the Kondo temperature is directly related to the magnetic exchange coupling, we conclude that the impurity–superconductor coupling decreases with decreasing tip–sample distance (that is, increasing junction conductance). Physically, the impurity is pulled away from the tip by the attractive atomic forces of the approaching sample substrate³⁴. This has been observed in a number of different experiments on YSR states introducing a tunability of the YSR energy^{27,28,32–34}.

The supercurrent, which is carried by tunnelling Cooper pairs (Josephson effect), is visible throughout the range of conductance values (Fig. 1e, red arrow). In the dynamical Coulomb

blockade (DCB) regime, in which the STM operates³⁶, the typical voltage-biased measurement shows a negative current peak followed by a positive current peak of equal size near zero bias voltage. The evolution of the Josephson effect as a function of conductance is shown in Fig. 2a. Each spectrum is shown in a bias voltage range of $\pm 60 \mu\text{eV}$ and offset horizontally. Assuming a harmonic current–phase relation in the DCB (that is, $I(\varphi) = I_C \sin \varphi$, where I_C is the critical current), the Josephson current is predicted to scale with the square of the critical current (Supplementary Section C), that is, $I(V) \propto I_C^2 \propto G_N^2$ (refs. 37–40). It can be directly seen in the data that this square dependence is not fulfilled in the dataset in Fig. 2a. In particular, the region indicated by the horizontal bracket shows notable deviations, even a slight decrease in the Josephson current with increasing conductance. The conductance at which the QPT occurs is indicated by a vertical dashed line, which falls directly into the region of the horizontal bracket.

For a more quantitative analysis we plot the current maxima I_S (switching current) for each conductance as a blue line in a double logarithmic plot in Fig. 2b. The expected square dependence on the conductance ($I_S \propto I_C^2 \propto G_N^2$) can be clearly seen for very small and very large conductances. In the transition region (indicated by the horizontal bracket), the behaviour of the switching current I_S strongly changes. For comparison, we plot the experimentally extracted energies of the YSR state (red line), which has a minimum at the QPT (vertical dashed line; see Methods for details). This indicates a drastic change in the behaviour of the Josephson effect across the QPT.

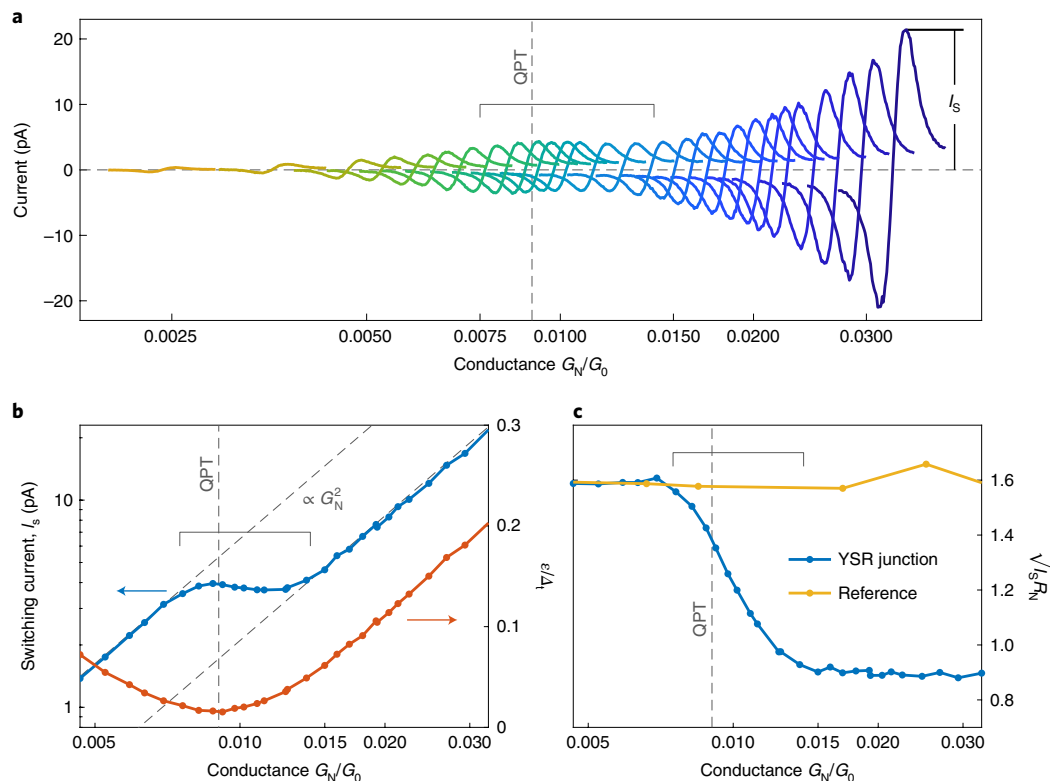


Fig. 2 | Josephson effect. **a**, Josephson spectra $I(V)$ in a range of $\pm 60 \mu\text{eV}$, shifted horizontally by the conductance at which they were measured. The horizontal bracket indicates the region where the evolution deviates from the conventional Ambegaokar-Baratoff formula. The QPT is indicated by the vertical dashed line. **b**, The switching current I_s , which is the current maximum indicated in **a** as function of the normal state conductance G_N (blue line). The square dependence at low and high conductance is indicated by dashed lines (labelled $\propto G_N^2$). The YSR energy as a function of conductance is shown as a blue line. The minimum indicates the QPT (vertical dashed line). The YSR state energy (red line) is plotted for comparison. The minimum indicates the QPT. **c**, $\sqrt{I_s}R_N$ (blue line) of the data in **b**, which is proportional to $I_c R_N$ for a harmonic energy-phase relation (R_N , renormalized resistance (see text); I_c , critical current). A reference junction without any YSR states is shown as an orange line, indicating the expected evolution according to the Ambegaokar-Baratoff formula.

To put the evolution of the switching current in reference to other Josephson junctions, we calculate $\sqrt{I_s}R_N$, which is shown in Fig. 2c (R_N is the normal state tunnelling resistance). This quantity is proportional to the product $I_c R_N$ for a harmonic energy-phase relation. In this way, the overall conductance dependence is eliminated such that the measurement appears like a step in Fig. 2c, with a sizeable reduction in height almost by a factor of two across the QPT. We will show in the following that this is due to a supercurrent reversal in the YSR channel, which leads to a crossover from a constructive to a destructive interference between the two transport channels.

To compare the experimental data to the theory, we have to renormalize the normal state resistance R_N for the YSR spectra due to the enhanced density of states from Kondo correlations (Supplementary Section D). The reference spectra (Fig. 2c, orange line) are measured for a Josephson junction without any YSR states—the $\sqrt{I_s}R_N$ is constant, as expected from the Ambegaokar-Baratoff formula^{41–43}.

To understand the behaviour of the Josephson effect in Fig. 2, the most convincing and consistent explanation is to assume the presence of a second transport channel that does not pass through a YSR state (BCS channel) and, therefore, is phase-insensitive. In fact, even a weak residual BCS channel is sufficient to provide a consistent analysis of our data. Thus, we first have a look at the energy-phase relations far away from the QPT at high and low conductance. In Fig. 3a, the energy-phase relations for the BCS channel and the YSR channel, which are calculated from a mean field Anderson impurity model (Supplementary Section E) and a non-selfconsistent

order parameter (Supplementary Section F), are shown in red and blue, respectively. To calculate the energy-phase relation, we apply a constant phase difference φ across the tunnel junction, but no bias voltage. A Fourier expansion of the energy-phase relation reveals that the most relevant contribution to the Josephson effect is the harmonic term proportional to $\cos(\varphi)$. Zooming in to both channels (cf. Fig. 3b), we estimate that the ratio of the channel transmissions is about 4:1 (YSR:BCS). This results in a significantly smaller amplitude for the energy-phase relation of the BCS channel (red) than in the YSR channel (blue) (Fig. 3b, ‘Individual channels’). The coherent superposition of these two channels (Fig. 3b, ‘Channel sum’) leads to an overall sign change, as well as different amplitudes, when the channels are in phase (Fig. 3b, upper row) or out of phase (Fig. 3b, lower row). In the measurement, we are only sensitive to the change in amplitude $I(V) \propto (E_{\text{YSR}} + 2E_{\text{BCS}})^2$ though, which results in the obvious step in Fig. 2c. We attribute the width of the step to the finite temperature in our experiment.

Because the temperature in our experiment (10 mK) is still non-zero, we expect fluctuations due to thermal excitations close to the QPT. The probability for the system to be in the ground state (blue) or the excited state (orange) is indicated in Fig. 3c using an effective temperature of 75 mK. This will broaden the expected sharp features associated with the quantum phase transition. Taking the excitation probability due to the finite temperature into account, we can calculate the expected Josephson current in the DCB regime (Supplementary Section G). The fit is shown in Fig. 3d, which shows excellent agreement with the data. The only free parameters

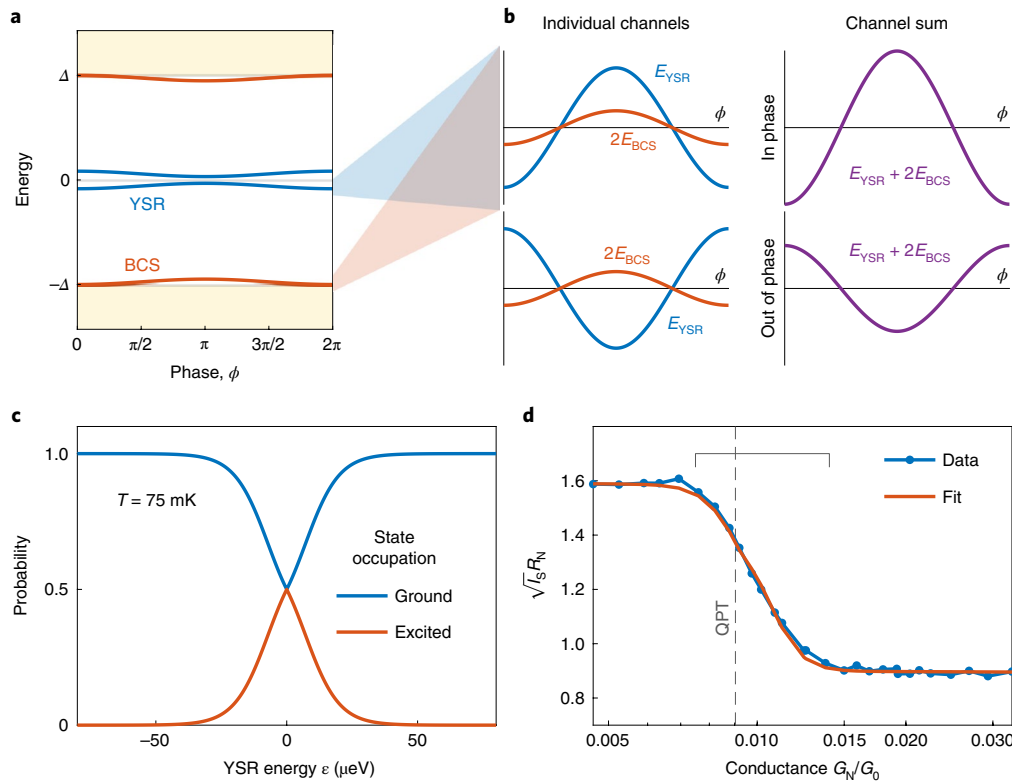


Fig. 3 | Supercurrent reversal. **a**, Energy-phase relation for the BCS channel (red) and the YSR channel (blue). For the Josephson current only the oscillation is relevant, but not the energy offset. **b**, A zoom-in to the oscillation for the two channels. The upper two panels in **b** show the in-phase oscillation in the screened spin regime. The lower two panels in **b** show the out-of-phase oscillation in the free spin regime, which is indicative of the supercurrent reversal. The STM is not sensitive to the sign of the supercurrent, but the concomitant change in magnitude is clearly observable. **c**, Probabilities for the system to be in the ground state (blue) or the excited state (red) as a function of YSR state energy. **d**, The $\sqrt{I_S}R_N$ product comparing experimental data with a theoretical fit. The only free parameters are the temperature, which defines the width of the QPT, and the relative channel transmission, which defines the step height.

are the effective temperature $T_{\text{eff}} = 75$ mK, which is determined by the width of the transition, and the ratio of the two channel transmissions, which is determined by the step height. For a best fit, we find that the YSR channel contributes 78.4% and the BCS reference channel contributes 21.6% to the total conductance relevant to the Josephson effect, which is consistent with the prominent YSR states and the strongly reduced coherence peaks in the quasiparticle spectra (Fig. 1e). All other parameters are given by the experimentally extracted values. In this way, we demonstrate that the supercurrent through an atomic-scale YSR state reverses on crossing the QPT, which can be detected in the STM by means of a BCS reference channel, in analogy to a SQUID geometry (for other YSR tips see Supplementary Section H).

To better understand the origin of this supercurrent reversal and to illustrate the crucial role of the impurity spin, we discuss the Cooper pair tunnelling process in Fig. 4 using the excitation picture. Zero energy denotes the ground state, ϵ is the energy of the excited YSR state and Δ marks the beginning of the quasiparticle continuum. The order is given by the numbered red arrows. Figure 4a describes the free spin regime, where the total spin is $S_{\text{tot}} = \frac{1}{2}$ (refs. 22,25). The Cooper pair transfer process involves a swap between two fermions, one associated with the impurity and one associated with the Cooper pair, as depicted by arrows 3 and 4 in Fig. 4a. Formally, this appears as an exchange of fermion operators inducing a negative sign (π shift)^{15,44}. By contrast, Fig. 4b shows the screened spin regime, which has a ground state with total spin $S_{\text{tot}} = 0$. Here the Cooper pair transfers conventionally, as in an empty BCS gap, except that the YSR state is used as an intermediate

(virtual) state instead of the continuum. It is this switching between transport regimes when crossing the QPT that we observe experimentally. Recalling from Fig. 1f that the impurity-substrate coupling reduces on increasing the conductance, we move from the screened spin regime across the QPT to the free spin regime as the tip approaches the sample. This is consistent with the evolution of the Josephson current from an in-phase superposition (zero junction) to an out-of-phase superposition (π -junction) as the conductance increases.

At the QPT, a system typically becomes very sensitive to external parameters, such as temperature. Here we note that the width of the QPT step in Fig. 3d depends only on temperature, but experiences no broadening from voltage noise. This is in contrast to conventional scanning tunnelling spectroscopy, where temperature broadening is typically obscured by voltage noise as well as interactions with the environment³⁶. Hence, YSR-tip functionalization may open new developments for low-temperature thermometry with high spatial resolution, where measuring the slope of the QPT step accesses the temperature (Supplementary Section I).

In summary, the experimental results directly reveal the consequences of the discrete parity change across the QPT in YSR states as well as the role of the impurity spin, which manifests itself in the supercurrent reversal. This allows for directly determining the ground state of the YSR state; that is, the supercurrent reveals whether the system is in the free or the screened spin regime. Our results establish an important connection to mesoscopic π -junctions, providing the perspective to transfer some of their concepts, for example, as sensing tools, to the atomic scale.

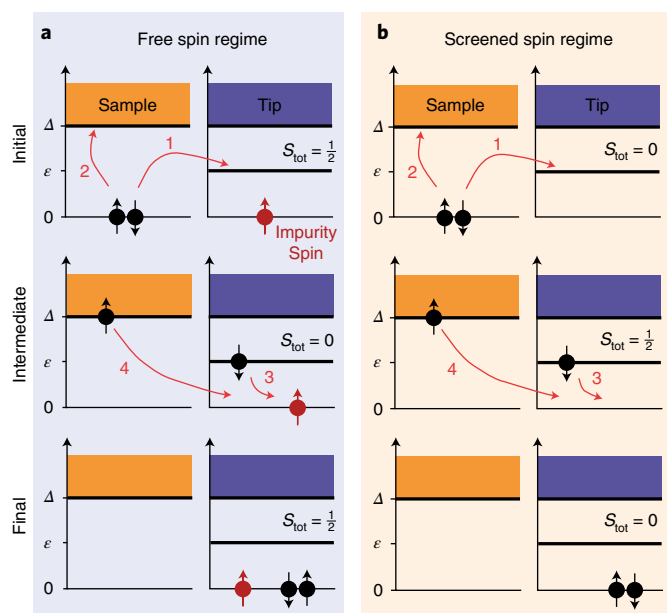


Fig. 4 | Cooper pair tunnelling. The tunnelling process in the free spin and screened spin regimes is shown from the initial to the final state via an intermediate (virtual) state in the excitation picture. The order is set by the numbered red arrows. The total spin S_{tot} describes the total spin of the YSR system, including the spin of the impurity. **a**, In the free spin regime, the order of the spins is exchanged compared to the initial state, which results in the supercurrent reversal. **b**, In the screened spin regime, the order of the spins is retained, such that there is no sign change in the supercurrent.

Having direct tunable access to the QPT could be exploited to enhance the sensitivity in quantum sensing applications, such as a local temperature measurement. Also, demonstrating the coherent superposition of different transport channels in the DCB regime introduces a rudimentary phase sensitivity in STM measurements that can be exploited in other scenarios as well, for example, in finding the symmetry of the superconducting order parameter.

Online content

Any methods, additional references, Nature Research reporting summaries, source data, extended data, supplementary information, acknowledgements, peer review information; details of author contributions and competing interests; and statements of data and code availability are available at <https://doi.org/10.1038/s41567-022-01644-6>.

Received: 8 September 2021; Accepted: 20 May 2022;

Published online: 4 July 2022

References

- Josephson, B. D. Possible new effects in superconductive tunnelling. *Phys. Lett.* **1**, 251–253 (1962).
- Kulik, I. Magnitude of the critical Josephson tunnel current. *J. Exp. Theor. Phys.* **22**, 841–843 (1966).
- Tsuei, C. C. et al. Pairing symmetry and flux quantization in a tricrystal superconducting ring of $\text{YBa}_2\text{Cu}_3\text{O}_{7-\delta}$. *Phys. Rev. Lett.* **73**, 593–596 (1994).
- Kirtley, J. R. et al. Symmetry of the order parameter in the high- T_c superconductor $\text{YBa}_2\text{Cu}_3\text{O}_{7-\delta}$. *Nature* **373**, 225–228 (1995).
- Van Harlingen, D. J. Phase-sensitive tests of the symmetry of the pairing state in the high-temperature superconductors—evidence for $d_{x^2-y^2}$ symmetry. *Rev. Mod. Phys.* **67**, 515–535 (1995).
- Wollman, D. A., Van Harlingen, D. J., Giapintzakis, J. & Ginsberg, D. M. Evidence for $d_{x^2-y^2}$ pairing from the magnetic field modulation of $\text{YBa}_2\text{Cu}_3\text{O}_{7-\delta}$ Josephson junctions. *Phys. Rev. Lett.* **74**, 797–800 (1995).
- Tsuei, C. C. & Kirtley, J. R. Pairing symmetry in cuprate superconductors. *Rev. Mod. Phys.* **72**, 969–1016 (2000).
- Gingrich, E. C. et al. Controllable 0- π Josephson junctions containing a ferromagnetic spin valve. *Nat. Phys.* **12**, 564–567 (2016).
- Cleuziou, J.-P., Wernsdorfer, W., Bouchiat, V., Ondarcuhu, T. & Monthiou, M. Carbon nanotube superconducting quantum interference device. *Nat. Nanotechnol.* **1**, 53–59 (2006).
- Feofanov, A. K. et al. Implementation of superconductor/ferromagnet/superconductor π -shifters in superconducting digital and quantum circuits. *Nat. Phys.* **6**, 593–597 (2010).
- Ryazanov, V. V. et al. Coupling of two superconductors through a ferromagnet: evidence for a π junction. *Phys. Rev. Lett.* **86**, 2427–2430 (2001).
- Kontos, T. et al. Josephson junction through a thin ferromagnetic layer: negative coupling. *Phys. Rev. Lett.* **89**, 137007 (2002).
- Robinson, J. W. A., Piano, S., Burnell, G., Bell, C. & Blamire, M. G. Critical current oscillations in strong ferromagnetic π junctions. *Phys. Rev. Lett.* **97**, 177003 (2006).
- Shimizu, Y., Horii, H., Takane, Y. & Isawa, Y. Multilevel effect on the Josephson current through a quantum dot. *J. Phys. Soc. Jpn* **67**, 1525–1528 (1998).
- van Dam, J. A., Nazarov, Y. V., Bakkers, E. P. A. M., De Franceschi, S. & Kouwenhoven, L. P. Supercurrent reversal in quantum dots. *Nature* **442**, 667–670 (2006).
- Estrada Saldaña, J. C. et al. Two-impurity Yu-Shiba-Rusinov states in coupled quantum dots. *Phys. Rev. B* **102**, 195143 (2020).
- Martín-Rodero, A. & Yeyati, A. L. Josephson and Andreev transport through quantum dots. *Adv. Phys.* **60**, 899–958 (2011).
- De Franceschi, S., Kouwenhoven, L., Schönberger, C. & Wernsdorfer, W. Hybrid superconductor-quantum dot devices. *Nat. Nanotechnol.* **5**, 703–711 (2010).
- Yu, L. Bound state in superconductors with paramagnetic impurities. *Acta Phys. Sin.* **21**, 75–91 (1965).
- Shiba, H. Classical spins in superconductors. *Prog. Theor. Phys.* **40**, 435–451 (1968).
- Rusinov, A. I. Superconductivity near a paramagnetic impurity. *JETP Lett.* **9**, 85–87 (1969).
- Salkola, M. I., Balatsky, A. V. & Schrieffer, J. R. Spectral properties of quasiparticle excitations induced by magnetic moments in superconductors. *Phys. Rev. B* **55**, 12648–12661 (1997).
- Flatté, M. E. & Byers, J. M. Local electronic structure of defects in superconductors. *Phys. Rev. B* **56**, 11213–11231 (1997).
- Flatté, M. E. & Byers, J. M. Local electronic structure of a single magnetic impurity in a superconductor. *Phys. Rev. Lett.* **78**, 3761–3764 (1997).
- Balatsky, A. V., Vekhter, I. & Zhu, J.-X. Impurity-induced states in conventional and unconventional superconductors. *Rev. Mod. Phys.* **78**, 373–433 (2006).
- Graham, M. & Morr, D. K. Imaging the spatial form of a superconducting order parameter via Josephson scanning tunneling spectroscopy. *Phys. Rev. B* **96**, 184501 (2017).
- Farinacci, L. et al. Tuning the coupling of an individual magnetic impurity to a superconductor: quantum phase transition and transport. *Phys. Rev. Lett.* **121**, 196803 (2018).
- Malavolti, L. et al. Tunable spin-superconductor coupling of spin 1/2 vanadyl phthalocyanine molecules. *Nano Lett.* **18**, 7955–7961 (2018).
- Franke, K. J., Schulze, G. & Pascual, J. I. Competition of superconducting phenomena and Kondo screening at the nanoscale. *Science* **332**, 940–944 (2011).
- Bauer, J., Pascual, J. I. & Franke, K. J. Microscopic resolution of the interplay of Kondo screening and superconducting pairing: Mn-phthalocyanine molecules adsorbed on superconducting Pb(111). *Phys. Rev. B* **87**, 075125 (2013).
- Kamlapure, A. et al. Correlation of Yu-Shiba-Rusinov states and Kondo resonances in artificial spin arrays on an s-wave superconductor. *Nano Lett.* **21**, 6748–6755 (2021).
- Huang, H. et al. Quantum phase transitions and the role of impurity-substrate hybridization in Yu-Shiba-Rusinov states. *Commun. Phys.* **3**, 199 (2020).
- Kezilebieke, S., Žitko, R., Dvorak, M., Ojanen, T. & Liljeroth, P. Observation of coexistence of Yu-Shiba-Rusinov states and spin-flip excitations. *Nano Lett.* **19**, 4614–4619 (2019).
- Ternes, M. et al. Interplay of conductance, force and structural change in metallic point contacts. *Phys. Rev. Lett.* **106**, 016802 (2011).
- Bork, J. et al. A tunable two-impurity Kondo system in an atomic point contact. *Nat. Phys.* **7**, 901–906 (2011).
- Ast, C. R. et al. Sensing the quantum limit in scanning tunnelling spectroscopy. *Nat. Commun.* **7**, 13009 (2016).
- Senkpiel, J. et al. Single channel Josephson effect in a high transmission atomic contact. *Commun. Phys.* **3**, 131 (2020).
- Ingold, G., Grabert, H. & Eberhardt, U. Cooper-pair current through ultrasmall Josephson junctions. *Phys. Rev. B* **50**, 395–402 (1994).
- Devoret, M. H. et al. Effect of the electromagnetic environment on the coulomb blockade in ultrasmall tunnel junctions. *Phys. Rev. Lett.* **64**, 1824–1827 (1990).

40. Averin, D., Nazarov, Y. & Odintsov, A. Incoherent tunneling of the cooper pairs and magnetic flux quanta in ultrasmall Josephson junctions. *Phys. B Condens. Matter* **165–166**, 945–946 (1990).
41. Jäck, B. et al. Critical Josephson current in the dynamical Coulomb blockade regime. *Phys. Rev. B* **93**, 020504 (2016).
42. Randeria, M. T., Feldman, B. E., Drozdov, I. K. & Yazdani, A. Scanning Josephson spectroscopy on the atomic scale. *Phys. Rev. B* **93**, 161115 (2016).
43. Ambegaokar, V. & Baratoff, A. Tunneling between superconductors. *Phys. Rev. Lett.* **10**, 486–489 (1963).
44. Spivak, B. I. & Kivelson, S. A. Negative local superfluid densities: the difference between dirty superconductors and dirty Bose liquids. *Phys. Rev. B* **43**, 3740–3743 (1991).

Publisher's note Springer Nature remains neutral with regard to jurisdictional claims in published maps and institutional affiliations.



Open Access This article is licensed under a Creative Commons Attribution 4.0 International License, which permits use, sharing, adaptation, distribution and reproduction in any medium or format, as long as you give appropriate credit to the original author(s) and the source, provide a link to the Creative Commons license, and indicate if changes were made. The images or other third party material in this article are included in the article's Creative Commons license, unless indicated otherwise in a credit line to the material. If material is not included in the article's Creative Commons license and your intended use is not permitted by statutory regulation or exceeds the permitted use, you will need to obtain permission directly from the copyright holder. To view a copy of this license, visit <http://creativecommons.org/licenses/by/4.0/>.
© The Author(s) 2022, corrected publication 2022

Methods

Tip and sample preparation. The experiments were performed on Josephson nanojunctions built in a low-temperature STM operated at 10 mK. Approaching a superconducting vanadium tip, tailored with a spin- $\frac{1}{2}$ impurity at its apex, to a crystalline V(100) substrate, we drove the impurity-induced YSR states across the QPT and detected a reversal of the supercurrent.

The V(100) substrate was cleaned by repeated cycles of Ar ion sputtering, annealing to ~ 925 K and cooling to ambient temperature at a rate of $1\text{--}2$ K s^{-1} . Oxygen diffused from the bulk to the surface leads to typical surface reconstructions^{45,46}; these did not influence the characteristics of the superconducting vanadium. Surface defects mostly involve missing oxygen within the reconstruction, which appeared bright in STM topographs⁴⁷. Magnetic defects were found exhibiting YSR states at arbitrary energies within the gap, as reported in ref. ⁴⁷.

The tip was sputtered in ultra-high vacuum and treated with field emission as well as subsequent indentation into the vanadium substrate until the expected gap of bulk vanadium appeared in the conductance spectrum. YSR tips were designed following the method of random dipping explained in ref. ⁴⁷. Although it is intrinsically not possible to know the exact composition of the tip apex, a probable scenario is that the YSR impurity on the tip consists of oxygen or carbon picked up from the surface in a way that leaves a free spin to interact with the superconductor. We purposefully chose to use YSR tips for our experiment as it gave better stability of the junction at higher conductance. Moreover, it offered better flexibility in designing and defining the junction over magnetic surface defects, which were mostly found to have a spatial extent of around 1 nm.

Extracting the superconducting gap. Experimentally, we extracted superconducting gaps for tip and sample of about $\Delta_t = \Delta_s = 725$ μeV (for the data in the main text). The crossing of the tip YSR state at the QPT is at $eV = \Delta_{\text{sample}}$ in the spectrum. The other gap Δ_{tip} can be extracted from the position of the coherence peaks ($\Delta_{\text{tip}} + \Delta_{\text{sample}}$) and the previously extracted Δ_{sample} .

We actually find a small gap of ~ 11 μeV at the YSR energy minimum, which is needed to properly fit the experimental data to the theoretical model. The existence of a small gap has actually been predicted in the context of a mean-field theory where the local variation of the order parameter close to the impurity was determined self-consistently⁴⁸. This was also reproduced in our self-consistent calculation in Supplementary Section F. As we find this small gap, we extract Δ_{sample} during the conversion of the YSR energies to the corresponding impurity–superconductor coupling, which we need for the modelling. The gap can be determined by the requirement that the impurity–superconductor coupling changes smoothly as function of conductance.

Theory. We modelled the Josephson effect in the dynamical Coulomb blockade regime. The interference between transport channels was calculated by a combination of the respective energy–phase relations. We exploited the concept of transport channels, which arise from the matrix diagonalization of the orbital overlap in the tunnel junction⁴⁹. This is a well-known procedure in mesoscopic physics and allows us to easily connect the theoretical models to experimentally accessible quantities without knowing all the microscopic details and, therefore, retaining a certain level of generality in the conclusions.

Our calculations of the Josephson effect were supplemented by self-consistent calculations of the local order parameter in a YSR state to verify that the experimentally observed step in the switching current across the QPT cannot be accounted for by a change in magnitude of the local order parameter, but must instead be attributed to the π shift of the phase in the YSR channel.

Furthermore, to extract the Kondo temperature from the experimental Kondo spectra at a magnetic field of $B = 1.5$ T, we used NRG theory to fit the experimental data⁵⁰.

Details for all the theoretical models are provided in the Supplementary Information.

Data availability

Data that support the plots within this paper and other findings of this study are available from the corresponding author upon reasonable request. Source data are available for this paper.

Code availability

The code that supports the conclusions within this paper and other findings of this study is available from the corresponding author upon reasonable request.

References

- Koller, R. et al. The structure of the oxygen induced (1×5) reconstruction of V(100). *Surf. Sci.* **480**, 11–24 (2001).
- Kralj, M. et al. HRAES, STM and ARUPS study of (5×1) reconstructed V(100). *Surf. Sci.* **526**, 166–176 (2003).
- Huang, H. et al. Tunnelling dynamics between superconducting bound states at the atomic limit. *Nat. Phys.* **16**, 1227–1231 (2020).
- Salkola, M. I., Balatsky, A. V. & Schrieffer, J. R. Spectral properties of quasiparticle excitations induced by magnetic moments in superconductors. *Phys. Rev. B* **55**, 12648–12661 (1997).
- Cuevas, J. C. & Scheer, E. *Molecular Electronics: an Introduction to Theory and Experiment* 2nd edn (World Scientific, 2017).
- Zitko, R. & Pruschke, T. Energy resolution and discretization artifacts in the numerical renormalization group. *Phys. Rev. B* **79**, 085106 (2009).

Acknowledgements

We gratefully acknowledge stimulating discussions with R. Drost, J. Fransson, B. Jäck and F. Tafuri. We dedicate this manuscript to the memory of F. Portier for the many inspirational discussions that the authors had with him. This work was funded in part by the ERC Consolidator Grant AbsoluteSpin (grant no. 681164; C.R.A.) and by the Center for Integrated Quantum Science and Technology (IQST). J.A. and C.P. acknowledge funding from the DFG under grant no. AN336/13-1, the IQST and the Zeiss Foundation. A.L.Y. and J.C.C. acknowledge funding from the Spanish Ministry of Science and Innovation (grant no. PID2020-117671GB-I00 and PID2020-114880GB-I00) and from the María de Maeztu Programme for Units of Excellence in Research and Development (grant no. CEX2018-000805-M). A.M.B.-S. acknowledges funding from the Knut and Alice Wallenberg Foundation through the Wallenberg Academy Fellows programme. Some of the computations were enabled by resources provided by the Swedish National Infrastructure for Computing (SNIC) at the High Performance Computing Center North (HPC2N) partially funded by the Swedish Research Council through grant agreement no. 2018-05973.

Author contributions

S.K. and H.H. conducted the experiments with support from K.K. and C.R.A. C.P., G.M., J.C.C., A.L.Y., B.K., A.T., A.M.B.-S. and J.A. provided theory support. H.H., C.P. and C.R.A. modelled and analysed the data with support from all authors. All authors discussed the results. C.R.A. wrote the manuscript with input from all authors.

Funding

Open access funding provided by Max Planck Society.

Competing interests

The authors declare no competing interests.

Additional information

Supplementary information The online version contains supplementary material available at <https://doi.org/10.1038/s41567-022-01644-6>.

Correspondence and requests for materials should be addressed to Christian R. Ast.

Peer review information *Nature Physics* thanks Andreas Heinrich and the other, anonymous, reviewer(s) for their contribution to the peer review of this work.

Reprints and permissions information is available at www.nature.com/reprints.